

August 2006

Catfish: A Monte Carlo simulator for black holes at the LHC

M. Cavaglià, R. Godang, L. Cremaldi and D. Summers

*Department of Physics and Astronomy
University of Mississippi
University, MS 38677-1848, USA*

Abstract

We present a new Fortran Monte Carlo generator to simulate black hole events at CERN’s Large Hadron Collider. The generator interfaces to the PYTHIA Monte Carlo fragmentation code. The physics of the BH generator includes, but not limited to, inelasticity effects, exact field emissivities, corrections to semiclassical black hole evaporation and gravitational energy loss at formation. These features are essential to realistically reconstruct the detector response and test different models of black hole formation and decay at the LHC.

Work supported in part by the U.S. Department of Energy contract DE-FG05-91ER40622.

Contents

1	Introduction	4
2	Basics of BH formation and evolution	4
2.1	BH formation and cross section at parton level	4
2.2	Cross section at nucleon level	5
2.3	BH evolution	6
3	BH generator	7
3.1	BH formation and parton cross section	7
3.2	Total and differential cross section	8
3.3	BH evaporation	8
3.4	BH final decay	9
3.5	Event simulation	10
4	Analysis of BH events	11
4.1	Black hole mass and missing energy	11
4.2	Sphericity, thrust and Fox-Wolfram moments	12
4.3	Heavy and light jet mass	13
5	Conclusions and further developments	13
6	Acknowledgments	15

List of Figures

1	M_{BH} , \cancel{E} , \cancel{E}_T and E_H for $M_\star = 1$ TeV and varying n	19
2	M_{BH} , \cancel{E} , \cancel{E}_T and E_H for $M_\star = 2$ TeV and varying n	20
3	M_{BH} , \cancel{E} , \cancel{E}_T and E_H for $n = 3$ and varying M_\star	21
4	M_{BH} , \cancel{E} , \cancel{E}_T and E_H for $n = 6$ and varying M_\star	22
5	M_{BH} , \cancel{E} , \cancel{E}_T and E_H for $M_\star = 1$ TeV, $n = 3$ and varying M_{min}	23
6	M_{BH} , \cancel{E} , \cancel{E}_T and E_H for $M_\star = 1$ TeV, $n = 6$ and varying M_{min}	24
7	M_{BH} , \cancel{E} , \cancel{E}_T and E_H for $M_\star = 1$ TeV, $n = 3$ and varying final BH decay mode.	25
8	M_{BH} , \cancel{E} , \cancel{E}_T and E_H for $M_\star = 1$ TeV, $n = 6$ and varying final BH decay mode.	26
9	M_{BH} , \cancel{E} , \cancel{E}_T and E_H for $M_\star = 1$ TeV, $n = 3$ and nonzero minimum length.	27
10	M_{BH} , \cancel{E} , \cancel{E}_T and E_H for $M_\star = 1$ TeV, $n = 6$ and nonzero minimum length.	28
11	R_2 , sphericity, thrust and number of jets for $M_\star = 1$ TeV, $n = 6$ and varying final BH decay mode.	29
12	Heavy and light jet mass for $M_\star = 1$ TeV, $n = 6$ and varying final BH decay mode. .	30

1 Introduction

The fundamental scale of gravity may be much lower than the measured gravitational scale [1]. In scenarios with large or warped extra dimensions, the observed weakness of gravity is explained by assuming that Standard Model (SM) fields are constrained to propagate on a four-dimensional submanifold, whereas gravitons propagate in the higher-dimensional spacetime [2]. If the gravitational coupling constant is of the order of few TeVs, super-Planckian events at CERN’s LHC could lead to the formation of subnuclear Black Holes (BHs) [3] and branes [4] (For reviews and further references, see Refs. [5, 6]).

The semiclassical limit of super-Planckian scattering suggests that the cross section for creation of a BH or brane with radius R is approximately equal to the geometrical Black Disk (BD) cross section $\sigma_{BD}(s, n) = \pi R^2(s, n)$, where \sqrt{s} is the Center of Mass (CM) energy of the colliding quanta and n is the number of extra dimensions. The semiclassical Hawking effect [7] provides a thermal decay mechanism for BHs, thus allowing their detection. The spectrum of massive excitations in string theories suggests that branes may also decay thermally [8]. Under the most favorable circumstances, the BH event rate at the LHC should be comparable to the $t\bar{t}$ event rate.

Until now, numerical studies of observational signatures have used Monte Carlo (MC) generators implementing the semiclassical picture outlined above. Currently, there are two MC generators for BH production at particle colliders: TRUENOIR [9] and CHARYBDIS [10]. However, recent results have modified significantly our understanding of BH formation and evolution. It is thus timely and worthwhile to examine the observational signatures of BH events beyond the simple semiclassical picture. To this purpose, we have developed a new Fortran MC generator for BH events at the LHC which includes many of the accepted theoretical results in the literature. The generator, called CATFISH (Collider grAviTational FIeld Simulator for black Holes), interfaces to the PYTHIA MC fragmentation code [11]. CATFISH allows the most accurate description of BH events at the TeV scale up-to-date. Its flexibility permits to compare the signatures of different theoretical models of BH production. MC generators with similar characteristics of CATFISH have already been successfully utilized to simulate BH production in ultrahigh-energy cosmic ray air showers [12] and in lepton colliders [13]. Precompiled executable versions of CATFISH (Linux and Mac OS platforms) are available at the CATFISH website <http://www.phy.olemiss.edu/GR/catfish>.

2 Basics of BH formation and evolution

In this section we follow Ref. [12] and briefly review the basics of BH formation and evolution.

2.1 BH formation and cross section at parton level

Thorne’s hoop conjecture [14] states that an event horizon forms when a mass M is compacted into a region with circumference smaller than twice the Schwarzschild radius $R(M)$ in any direction. At the LHC, this process can be achieved by scattering two partons ij with CM energy larger than M and impact parameter smaller b than R . The BH event is described by the inelastic process $ij \rightarrow \text{BH} + E(X)$, where $E(X)$ denotes the collisional energy that does not fall beyond the event horizon. Due to the gravitational nature of the process, this energy includes mainly a bulk component of gravitational radiation, although non-SM gauge fields and a brane component of SM fields cannot be excluded. If $E(X)$ is zero, the hoop conjecture implies that the parton cross section for BH production is equal to the geometrical BD cross section, $\sigma_{ij}(s, n) = \sigma_{BD}(s_{ij}, n)\theta(R(s_{ij}) - b)$.

If $E(X) \neq 0$, the cross section is generally smaller and depends on the impact parameter. Note that this treatment is valid only if the BH is larger than the Compton length of the colliding quanta. (For discussions on the effect of wave packet size on the BH formation process, see Refs. [15].) A precise calculation of the collisional energy loss is essential to understanding BH formation.

The hoop conjecture has been tested by different methods [6], the most popular one being the Trapped-Surface (TS) approach [16, 17, 18]. The TS model gives a bound on the inelasticity by modeling the incoming partons as two Aichelburg-Sexl shock waves [19]. The Aichelburg-Sexl wave is obtained by boosting the Schwarzschild solution to the speed of light at fixed energy. The resulting metric describes a plane-fronted gravitational shock wave corresponding to the Lorentz-contracted longitudinal gravitational field. The parton scattering is simulated by superposing two shock waves traveling in opposite directions. The union of these shock waves defines a closed TS that allows to set a lower bound on the initial BH mass M_{BH} . The collisional energy loss depends on the impact parameter and increases as the number of spacetime dimensions increases. The BH mass monotonically decreases with the impact parameter from a maximum of about 60-70% of the CM energy for head-on collisions.

The TS result is consistent within one order of magnitude with the hoop conjecture. However, this approach neglects mass, spin, charge and finite-size effects of the incoming partons. Size and spin effects are expected to be mostly relevant around the Planck energy. Charge effects could dominate at higher energy. The pointlike approximation fails for directions transversal to the motion [20]. Even with these assumptions, the TS model provides only a lower bound on M_{BH} . Independent estimates of the gravitational collisional energy loss are possible through alternative approaches. The gravitational energy emission in a hard instantaneous collision can be evaluated in the linearized limit [21]. This computation suggests that the TS method overestimates the gravitational energy emitted in the process. For head-on collisions, the instantaneous method predicts that the gravitational energy loss is only about 10% of the CM energy. This result is in agreement with perturbative calculations modeling the parton-parton collision as a plunge of a relativistic test particle into a BH with mass equal to the CM energy [22].

In conclusion, a conservative estimate of gravitational loss in relativistic scattering at parton level gives a BH mass ranging between 60% and 100% of the CM energy. The TS result and the BD result can be considered as the lower and upper bounds on M_{BH} , respectively.

2.2 Cross section at nucleon level

The total cross section for a super-Planckian BH event involving two nucleons is obtained by integrating the parton cross section over the Parton Distribution Functions (PDFs). If the BH mass depends on the impact parameter, the generally accepted formula for the total cross section of the pp process is

$$\sigma_{pp \rightarrow BH}(s, n) = \sum_{ij} \int_0^1 2z dz \int_{x_m}^1 dx \int_x^1 \frac{dx'}{x'} f_i(x', Q) f_j(x/x', Q) F \sigma_{BD}(xs, n), \quad (1)$$

where $f_i(\cdot, Q)$ are the PDFs with four-momentum transfer squared Q [23, 24] and z is the impact parameter normalized to its maximum value. The cutoff at small x is $x_m = M_{min}^2/(sy^2(z))$, where $y(z)$ and M_{min} are the fraction of CM energy trapped into the BH and the minimum-allowed mass of the gravitational object, respectively. F is a form factor. The total cross section for the BD model is obtained by setting $F = 1$ and $y^2(z) = 1$.

Different sets of PDFs are defined in the literature. The PDFs are not known at energies above the TeV and for values of momentum transfer expected in BH formation. Equation (1) is usually calculated by imposing a cut-off at these values. The PDFs also suffer from uncertainties at any momentum transfer ($\sim 10\%$) [25] and from the ambiguity in the definition of Q [26]. The momentum transfer is usually set to be M_{BH} or the Schwarzschild radius inverse. The uncertainty due to this ambiguity is about $\sim 10 - 20\%$.

The form factor and the amount of trapped energy depend in principle on energy, gravitational scale, geometry and physical properties of the spacetime. The TS method gives numerical values of order unity for these quantities. (See Refs. [16, 17] and discussion above). However, these results depend on the way the TS is identified. Other models [27] give values which are more or less consistent with the TS method. It is common practice in the literature to either choose the TS result or the simple BD model.

The lower cutoff on the fraction of the nucleon momentum carried by the partons is set by the minimum-allowed formation mass of the gravitational object, M_{min} . This threshold is usually considered to be roughly equal to the minimum mass for which the semiclassical description of the BH is valid. However, this argument is based on Hawking's semiclassical theory and may not be valid at energies equal to few times the Planck mass. For example, the existence of a minimum spacetime length l_m implies the lower bound on the BH mass [28, 29]:

$$M_{ml} = \frac{n+2}{8\Gamma\left(\frac{n+3}{2}\right)} \left(\sqrt{\pi} l_m M_\star / 2\right)^{n+1} M_\star. \quad (2)$$

BHs with mass less than M_{ml} do not exist, since their horizon radius would fall below the minimum-allowed length. Note that M_{ml} grows as a power of l_m^{n+1} at fixed M_\star . Therefore, M_{min} may be much larger than M_\star for higher-dimensional spacetimes.

2.3 BH evolution

It is believed that the decay of microscopic BHs happens in four distinct stages: I. radiation of excess multipole moments (balding phase); II. spin-down; III. Hawking evaporation; IV. final explosion or formation of a BH remnant.

Although some progress has been made, a quantitative description of the balding phase and the spin-down phase is not fully known. For example, the emission of radiation from a $(n+4)$ -dimensional rotating BH on the brane is not known for spin-2 fields [30]. Due to these limitations, balding phase and spin-down phase effects are not implemented in the current version of CATFISH. It should be stressed, however, that balding and spin-down effects could play an important role in BH phenomenology at the LHC.

Many papers have been devoted to the investigation of BH evaporation in higher dimensions [31], leading to a better understanding of the Hawking phase. Field emissivities for all SM fields have recently been calculated [32]. For non rotating BHs and the minimal $SU(3) \times SU(2) \times U(1)$ SM, most of the BH mass is radiated as SM quanta on the brane, although the gravitational emission in the bulk cannot be neglected for high n . Two points should be stressed [33]: (i) it is not clear what is the effect of rotation on BH emissivities; (ii) the field content at trans-Planckian energies is not known. Onset of supersymmetry, for example, could lead to other evaporation channels and large emission of undetectable non-SM quanta during the decay phase even in absence of rotation [34].

Quantum gravitational effects and BH recoil [35] could also affect the emission of visible quanta on the brane. Examples of quantum gravitational effects are quantum thermal fluctuations and

corrections to the Hawking thermodynamics due to the existence of a minimum length [29]. The existence of a minimum scale of the order of the Planck length [36] is a common consequence of most (if not all) theories of quantum gravity such as string theory, non-commutative geometry, canonical quantum gravity, etc. The presence of a cutoff at the Planck scale leads to a modification of the uncertainty principle. Since the Hawking thermodynamical quantities can be derived by applying the uncertainty principle to the BH, the existence of a minimum length leads to corrections in the thermodynamical quantities [28, 29].

At the end of the Hawking phase, the BH is expected to either non-thermally decay in a number n_p of hard quanta or leave a remnant. In either case, the lack of a theory of quantum gravity does not allow more than a phenomenological treatment. The final decay is usually described by setting a cutoff on the BH mass of the order of the Planck mass, $Q_{min} \sim M_*$, and equally distributing the energy Q_{min} to n_p quanta. Since the decay is non-thermal, and in absence of any guidance from a theory of quantum gravity, the quanta are democratically chosen among the SM Degrees of Freedom (DoFs). Note that Q_{min} does not necessarily coincide with M_{min} . The former gives the threshold for the onset of quantum gravity effects in the decay phase, whereas the latter gives the minimum-allowed mass of the classical BH in the formation process. From the above definitions, it follows $M_{min} \geq Q_{min}$. The existence of a minimum length gives a natural means to set Q_{min} . In that case, the modified thermodynamical quantities determine the endpoint of Hawking evaporation when the BH mass reaches M_{ml} . This mass can be identified with the mass of the BH remnant.

3 BH generator

In this section we list the main characteristics of the CATFISH generator. The physics of BH formation and decay is determined by the following set of external parameters and switches in the MC code:

- Fundamental Planck scale (M_*)
- Number of large extra dimensions (n)
- Gravitational loss at formation
- Gravitational loss model
- Minimum BH mass at formation (M_{min})
- Quantum BH mass threshold at evaporation (Q_{min})
- Number of quanta at the end of BH decay (n_p)
- Momentum transfer model in parton collision
- Conservation of electromagnetic (EM) charge
- Minimum spacetime length (α)

These parameters are briefly explained below.

3.1 BH formation and parton cross section

The MC generator does not require any lower or upper bound on the Planck mass M_* . However, experimental constraints exclude values of $M_* \lesssim 1$ TeV [37, 38] and BHs do not form at the LHC if $M_* > 14$ TeV. Models with one or two flat large extra dimensions are excluded experimentally [37, 38]. Most of the theoretical models are limited to $n \leq 7$. Therefore, the allowed number of extra dimensions n ranges from 3 to 7. (Warped scenarios such as the Randall-Sundrum models [39] with a single extra dimension are experimentally viable. However, the extra dimension is warped.

Since most of the results in the literature concerning black holes at colliders have been derived for a flat extra-dimensional scenario, we choose not to allow $n = 1$ to mimic BH production in warped models.)

CATFISH includes three models for BH formation and cross section: BD, Yoshino-Nambu (YN) TS model [16], and Yoshino-Rychkov (YR) improved TS model [17]. The minimum BH mass M_{min} is set in units of M_\star or, if a minimum length is present, M_{ml} : $X_{min} = M_{min} \geq \text{Max}(M_\star, M_{ml})$. This parameter is always larger than one.

3.2 Total and differential cross section

The distribution of the initial BH masses is sampled from the differential cross section $d\sigma/dM_{BH}$. CATFISH uses the (stable) cteq5 PDF distribution [23, 40]. The use of different PDF distributions should not significantly affect the total and differential cross sections. Therefore, different PDF distributions are not implemented in the code. The uncertainty due to the choice of the momentum transfer is generally larger. A logical switch allows a choice between M_{BH} or inverse Schwarzschild radius, as the definition of momentum transfer. The part of CM energy of the pp collision which is not trapped or lost in gravitational radiation at formation is attributed to the beam remnant. This remnant is considered lost in the beam pipe due to its small transverse momentum and is not injected in PYTHIA.

3.3 BH evaporation

Due to the lack of results for the balding and spin-down phases described above, energy losses in these stages are assumed to be either negligible or included in the energy loss during formation. Since the TS model likely overestimates the actual energy loss, this is a reasonable assumption. However, we stressed above that balding and spin-down effects could significantly affect the event signatures. We plan to include balding and spin-down effects in updated versions of the code, as soon as theoretical results become available.

A similar approach is used in the Hawking phase, where the MC uses only the emissivities of non-rotating spherically-symmetric BHs [32]. (Emissivities for rotating BHs are not fully known.) This is a reasonable assumption, given that the BH is expected to be bald and spinless by the time the evaporation phase begins. Moreover, intrinsic uncertainties in event reconstruction should hide at least some of the differences between rotating and non-rotating field emissivities. The particle content at trans-Planckian energy is assumed to be the minimal $SU(3) \times SU(2) \times U(1)$ SM with three families and a single Higgs boson on a thin brane. For black holes with mass \sim few TeV the Hawking temperature is generally above 100 GeV. Therefore, all SM DoFs can be considered massless. (Considering massive gauge bosons does not affect the conclusions significantly.) The spin-0, -1/2 and -1 DoFs on the brane are 1 (Higgs field), 90 (quarks + charged leptons + neutrinos) and 27 (gauge bosons), respectively. The longitudinal DoFs of the weak bosons are included in the counting. The DoFs c_i and the relative emissivities $\Gamma_{\mathcal{P}_i}$ and $\Gamma_{\mathcal{R}_i}$ [32] are given in Table I – III, respectively. In the notations of Ref. [32] the total decay multiplicity is [33]

$$N = \frac{(n+1)S}{4\pi} \frac{\sum_i c_i \mathcal{R}_i \Gamma_{\mathcal{R}_i}}{\sum_j c_j \mathcal{P}_j \Gamma_{\mathcal{P}_j}}, \quad (3)$$

where S is the initial entropy of the BH and the emissivity normalizations for spin- s fields are:

$$\mathcal{P}_s = \begin{cases} 2.9 \times 10^{-4} & s = 0 \\ 1.6 \times 10^{-4} & s = 1/2 \\ 6.7 \times 10^{-5} & s = 1 \\ 1.5 \times 10^{-5} & s = 2 \end{cases}, \quad \mathcal{R}_s = \begin{cases} 1.4 \times 10^{-3} & s = 0 \\ 4.8 \times 10^{-4} & s = 1/2 \\ 1.5 \times 10^{-4} & s = 1 \\ 2.2 \times 10^{-5} & s = 2 \end{cases}. \quad (4)$$

The decay multiplicities per species N_i are

$$N_i = N \frac{c_i \mathcal{R}_i \Gamma_{\mathcal{R}_i}}{\sum_j c_j \mathcal{R}_j \Gamma_{\mathcal{R}_j}}. \quad (5)$$

The presence of a minimum length affects the evaporation phase. CATFISH uses the dimensionless parameter $\alpha = l_m M_\star/2$ to determine the minimum length. If there is no minimum length, i.e. $\alpha = 0$, the MC evaporates the BH according to the Hawking theory (with varying temperature). Alternatively, the BH evolution proceeds according to the modified thermodynamics of Ref. [28, 29]. In both cases the evaporation ends when the BH reaches the mass Q_{min} . This is set in units of M_\star (M_{ml}) if the minimum length is zero (nonzero). Note that the BH minimum formation mass M_{min} and the endpoint of Hawking evaporation Q_{min} are independent parameters.

Four-momentum is conserved at each step in the evaporation process by taking into account the recoil of the BH on the brane due to the emission of the Hawking quanta. The initial energy of the BH is distributed democratically among all the Hawking quanta with a random smearing of $\pm 10\%$. This smearing factor is introduced on a purely phenomenological basis to take into account quantum uncertainties in the emission of each quantum.

3.4 BH final decay

The MC code allows for two different choices of final BH decay: Final explosion in a number n_p of quanta or BH remnant. If $n_p = 0$, the BH settles down to a remnant with mass Q_{min} . If $n_p = 2 \dots 18$, the BH decays in a number n_p of quanta by a n -body process with total CM energy equal to Q_{min} .

A logical switch controls conservation of EM charge in the decay process (Hawking evaporation + final decay). The purpose of this switch is to allow for the existence of a charged or neutral BH remnant.

If the EM charge switch is set to **FALSE**, there is no constraint on the total charge of the emitted quanta Q_E . If $n_p = 0$, physical charge conservation implies the relation $Q_E + Q_R + Q_B = 2e$, where Q_E is the total charge of the Hawking quanta, Q_R is the charge of the BH remnant and Q_B is the charge of the beam remnant. In that case, the BH remnant can be either neutral or charged, depending on the event. The choice $n_p \neq 0$ and no charge conservation (**FALSE**) is unphysical and should be avoided.

If the EM charge switch is set to **TRUE**, the absolute value of the total charge of the emitted quanta is $|Q_E| \leq 4e/3$, i.e. the maximum possible total charge of the scattering partons. In that case, the excess charge $2e - Q_E$ is assigned to the beam remnant and, if $n_p = 0$, the BH remnant is considered neutral. This is justified from the fact that the BH charge should have been shed earlier in the evaporation process. (See, however, Ref. [41] for a different viewpoint.) It should be stressed that the collider phenomenology of a charged remnant is not known and it is not clear how to track it in a detector in a meaningful way.

	c_i
Quarks	72
Charged leptons	12
Neutrinos	6
Photon	2
EW bosons	9
Gluons	16
Higgs	1
Graviton	1

Table 1: DoFs c_i for the SM fields on a thin brane. The graviton is assumed to propagate in all $(n+4)$ dimensions. Following Ref. [32], the $(n+4)(n+1)/2$ graviton helicities are included in the emissivities (see Table 2 and 3 below). Therefore, the graviton counts as one DoF. Longitudinal DoFs are included in the EW boson counting.

	n=3	n=4	n=5	n=6	n=7
Higgs	1	1	1	1	1
Fermions	0.89	0.87	0.85	0.84	0.82
Gauge Bosons	1.0	1.04	1.06	1.06	1.07
Gravitons	2.7	4.8	8.8	17.7	34.7

Table 2: Fraction of radiated power per DoF and species i , $\Gamma_{\mathcal{P}_i}$, normalized to the Higgs field. The graviton values include all the helicity states. (From Ref. [32].)

	n=3	n=4	n=5	n=6	n=7
Higgs	1	1	1	1	1
Fermions	0.78	0.76	0.74	0.73	0.71
Gauge Bosons	0.83	0.91	0.96	0.99	1.01
Graviton	0.91	1.9	2.5	5.1	7.6

Table 3: Fraction of emission rates per DoF and species i , $\Gamma_{\mathcal{R}_i}$, normalized to the Higgs field. The graviton values include all the helicity states. (From Ref. [32].)

3.5 Event simulation

The steps to simulate a BH event are:

1. The initial BH mass in the CM frame is sampled from the differential cross section.
2. The BH is decayed through the Hawking mechanism and final hard event.
3. The unstable quanta from the BH are hadronized or decayed instantaneously by PYTHIA, with the exception of top quarks. These are instantaneously decayed as $t \rightarrow bW$ before being injected in PYTHIA.

4 Analysis of BH events

Signatures of BH events at the LHC have been investigated in a number of papers [42, 43, 44, 45, 46, 47] using the TRUENOIR [9] or CHARYBDIS [10] generators. In this section we present some results for CATFISH. We focus on a purely statistical analysis of variables which allow an easy comparison with previous results obtained with the CHARYBDIS generator. A more refined analysis of other detector response-dependent signatures such as back-to-back di-jet suppression, di-lepton events ($\mu^+\mu^-$, μ^+e^- , μ^+e^+ , ...) will be presented in a future publication [48].

4.1 Black hole mass and missing energy

Missing energy (\cancel{E}), missing transverse energy (\cancel{E}_T) and hadron energy (E_H) are important signatures of BH production in particle colliders. Figure 1 shows the simulation output for 10,000 events at the LHC with the following parameters:

$$M_\star = 1 \text{ TeV}, \quad M_{min} = 2M_\star, \quad Q_{min} = M_\star, \quad n_p = 2, \quad \alpha = 0$$

and conservation of EM charge. The momentum transfer is set to be equal to the Schwarzschild radius inverse. (This choice of momentum transfer applies to all simulations throughout the paper.) The plots show the initial BH mass distribution (M_{BH}), \cancel{E} , \cancel{E}_T and E_H for the BD model and the TS model (YR approach) with varying number of extra dimensions $n = 3 \dots 6$. Figure 2 shows the results for a higher value of the fundamental Planck mass ($M_\star = 2 \text{ TeV}$).

The plots in Figs. 1 and 2 for the BD model can be used to compare CATFISH with previous BH generators. For example, the BD missing transverse energy distributions are in good agreement with results obtained with CHARYBDIS [43]. BH events show a large amount of missing energy and missing transverse energy up to several TeV, depending on the value of the fundamental scale and other parameters of the model. In the absence of a BH remnant, the missing energy is due to gravitons during the process of BH formation (YR model only) and undetectable quanta (gravitons and neutrinos) during the evaporation phase, the former process being the dominant contribution. Detectable quanta are originated in the Hawking and final decay phase with an upper bound to their multiplicity given by Eq. (3). Since the bulk of BH events is characterized by light, low-entropy BHs, only a small amount of initial BH energy can actually be detected on average. The BH radiates gravitons uniformly on the visible brane. Therefore, the missing transverse energy provides an estimate for energy loss in gravitons and neutrinos during the evaporation+final decay phase. The plots show that this energy is generally (approximately) less than $2M_\star$. This indicates that for TeV BHs, neutrino and graviton emission in the decay phase accounts only for a small fraction of the total multiplicity, as it is expected from a rough counting of DoF.

Changing the number of extra dimensions does not affect significantly the BH mass and the missing and visible energy outputs; effects due to the dimensionality of spacetime are more evident for massive BHs, whereas most of the BHs produced at the LHC are very light. Therefore, it is likely that LHC would not be able to determine the number of extra dimensions just by statistical means. Detection of gravitational emission stands a better chance. Comparison of BD and YR outputs shows that the missing energy in the latter model is significantly higher than in the former. The difference is given by gravitational emission during the formation process. Gravitational energy loss during this phase does not depend on other parameters of the model, thus its effects can be easily disentangled. For example, the transverse missing energy is due to the decay phase and is essentially unaffected by the initial gravitational emission.

Figures 3 and 4 show how the value of the fundamental scale affects M_{BH} , \mathcal{E} , \mathcal{E}_T and E_H . Increasing M_\star leads to higher M_{min} and more massive BHs, i.e., a higher multiplicity and harder quanta in the Hawking phase. The overall effect is larger \mathcal{E}_T (more invisible hard quanta are emitted in the Hawking phase) and smaller \mathcal{E} (less CM energy is initially released in gravitational waves). The plots show that different fundamental scales produce significantly different outputs. Observation of events with $\mathcal{E}_T \gtrsim 3$ TeV would indicate a value of M_\star larger than 2 TeV, independently of the details of BH formation and the number of extra dimensions. If BHs are observed at the LHC, it is thus conceivable that M_\star could be measured to a certain degree of precision.

Figures 5 and 6 show the effects of varying the minimum mass lower bound. A measure of M_{min} at the LHC on purely statistical basis seems to be difficult. Effects due to changes in M_{min} are entangled with effects due to the initial graviton emission. This can be explained as follows: In the BD model, larger values of M_{min} (at fixed M_\star) lead to more massive BHs, and thus to higher \mathcal{E}_T . However, if the initial gravitational emission is turned on, this increase may be balanced by a decrease due to lower multiplicity in the Hawking phase.

Figures 7 and 8 display the effects of the final BH decay. The initial BH mass distribution is obviously unaffected by the details of the final decay. (The M_{BH} plot provides a consistency check for the code.) The \mathcal{E} , \mathcal{E}_T and E_H plots show that it is virtually impossible to distinguish the $n_p = 2$ model from the $n_p = 4$ model. Although quanta emissivities in the Hawking phase and the final phase differ for the presence of greybody factors in the former, the difference in \mathcal{E} and \mathcal{E}_T is not sufficient to allow a separation without a spectral analysis of the energy and the number of emitted quanta (more and softer quanta are expected for larger n_p , see Sec. 4.3). The detection of a BH remnant stands a better chance because of larger \mathcal{E} and smaller E_H due to its undetectability. (See also Refs. [41, 42].) Note that a large fraction of events with remnant does not produce any visible output. This is due to the fact that most of the BHs are initially so light that the Hawking phase does not take place. For higher mass events, the energy carried by the decay products is much larger than the invisible energy carried by the remnant. Therefore, detection of a remnant is less likely in high-mass events.

Figures 9 and 10 compare M_{BH} , \mathcal{E} , \mathcal{E}_T and E_H for a smooth spacetime ($\alpha = 0$) and a spacetime with nonzero minimum length equal to the fundamental Planck scale inverse ($\alpha = 0.5$). The plots show no significant statistical differences between the two cases. The effects of a small distance cut-off becomes only relevant when the minimum scale is very close to the threshold of complete suppression of BH production, i.e., when the minimum allowed mass Eq. (2) is so large that BHs cannot form at the LHC CM energy. Therefore, observation of minimum length effects at the LHC requires a certain degree of fine tuning in the parameter α . It is unlikely that any information on quantum effects at the Planck scale can be extracted from the data on a statistical basis.

4.2 Sphericity, thrust and Fox-Wolfram moments

BH events are expected to be highly spherical because of the spherical nature of Hawking evaporation. The event shape can be quantified by means of the sphericity S [49], thrust T [50], and Fox-Wolfram moment [51] $R_1 \dots R_4$ variables. The first three panels of Fig. 11 show the second Fox-Wolfram moment, sphericity and thrust for

$$M_\star = 1 \text{ TeV}, \quad n = 6, \quad M_{min} = 2M_\star, \quad Q_{min} = M_\star, \quad \alpha = 0,$$

BD and TS models and different final decay modes ($n_p = 2, 4$), respectively. (Rare) massive BH events are characterized by very high sphericity: $R_2 \lesssim 0.25$, $S \gtrsim 0.75$ and $T \sim 0.5$. Comparison

between BD and TS models at fixed n_p shows that the BD model leads to more spherical events. This is expected because BD BHs are on average more massive and emit more quanta in the Hawking phase (see fourth panel) than TS BHs. The higher sphericity of BD events is evident from the distribution tails, where massive events are displayed. In that case, Hawking emission dominates emission in the final explosive phase, making the statistical difference between BD and TS models more clear. Comparison between $n_p = 2$ and $n_p = 4$ at fixed BD or TS shows that the former events are less spherical than the latter. This is clearly displayed in the region of the plots corresponding to light BHs, where emission in the final phase dominates over Hawking emission. However, it should be stressed that the distinction between $n_p = 2$ and $n_p = 4$ at the LHC might well prove impossible due to the presence of non-BH background (e.g. $q\bar{q}$ events). On the contrary, distinction between BD and alternative models of BH formation should be possible by selecting massive spectacular events with high sphericity. Safe conservative cuts for a meaningful analysis are ($R_2 \leq 0.75$, $S \geq 0.25$ and $T \leq 0.8$).

4.3 Heavy and light jet mass

Figure 12 shows heavy and light jet mass [11] for the choice of parameters discussed above. Both plots display a discontinuity at 1 TeV, corresponding to Q_{min} . This discontinuity essentially separates jets that are originated in the final decay phase (jet mass < 1 TeV) from jets emitted during the Hawking phase (jet mass > 1 TeV). We have seen that the BD model produces on average BHs more massive than the TS model. This is evident from the right portions of the jet mass distributions, where the BD model is characterized by more massive jets than the TS model at fixed n_p . Therefore, measurement of hard jet mass allows a determination of the BH formation model independent of the shape variables. On the other hand, the measurement of low jet mass (left portions of the plots) may give important information on the physics of the final BH phase.

5 Conclusions and further developments

The study of BH production at the TeV scale is now a few years old and entering the mature stage. Although some of the characteristics of subatomic BH production remain obscure, many new theoretical results have been published in the literature. A MC generator which includes these theoretical results is needed for accurate simulations of BH events at the forthcoming LHC. Such a generator is also important to check the stability of the overall picture of BH production against improvements in the theory and have independent confirmation of previous results obtained with existing generators. With this in mind, we have developed CATFISH. The CATFISH generator implements several features of BH production at the TeV scale which were not included in TRUENOIR and CHARYBDIS. CATFISH new physics includes inelasticity effects during the BH formation phase [16, 17], exact field emissivities (albeit only for non-rotating BHs) [32], corrections to Hawking's semiclassical evaporation phase [28, 29], BH recoil on the brane, and different final BH decay modes with possibility of remnant formation [41]. These features allow the most accurate description of BH events at the TeV scale up-to-date. Another important feature of CATFISH is its flexibility. CATFISH design based on independent subroutine blocks allows easy inclusion of new theoretical results as soon as they become available. For example, the most significant changes to the phenomenology of BH formation in particle colliders is expected to arise from spin and charge effects. Emissivities for rotating and/or charged BHs can be easily implemented in CATFISH if known. We are also planning to include in future versions of the MC generator backreaction effects

during the Hawking phase (see, e.g., Ref. [44]), thermodynamic fluctuations [29], SUSY effects [34] and photosphere and chromosphere effects [52].

The analysis of BH formation presented in the second part of this paper is limited to a few statistical observables. This represents by no means CATFISH full potentiality. Several other interesting signatures of BH formation in particle colliders have been investigated in the literature (see, e.g., Refs. [42, 43, 45, 46, 47]). In particular, suppression of high-energy back-to-back-correlated di-jets with energy above the fundamental scale and di-lepton production with large transverse momentum are expected to be two of the most interesting signatures of BH production at the LHC. Investigation of these signatures with CATFISH is in progress [48]. Finally, detector response and event reconstruction are also fundamental issues to be addressed in a complete analysis of BH events at the LHC. Further work along these lines is currently being pursued. Precompiled executable Linux and Mac OS versions of CATFISH can be downloaded at the CATFISH website: <http://www.phy.olemiss.edu/GR/catfish>.

6 Acknowledgments

The authors would like to thank Vitor Cardoso, David Cline, Greg Landsberg, Alexander Melnitchouk, Robert Palmer, Hans Wenzel and Graham Wilson for discussions and many useful suggestions. This work was supported in part by the U.S. Department of Energy contract DE-FG05-91ER40622.

References

- [1] N. Arkani-Hamed, S. Dimopoulos and G. R. Dvali, Phys. Lett. B **429**, 263 (1998) [arXiv:hep-ph/9803315]; I. Antoniadis, N. Arkani-Hamed, S. Dimopoulos and G. R. Dvali, Phys. Lett. B **436**, 257 (1998) [arXiv:hep-ph/9804398]; N. Arkani-Hamed, S. Dimopoulos and G. R. Dvali, Phys. Rev. D **59**, 086004 (1999) [arXiv:hep-ph/9807344].
- [2] R. Maartens, Living Rev. Rel. **7**, 7 (2004) [arXiv:gr-qc/0312059].
- [3] T. Banks and W. Fischler, arXiv:hep-th/9906038; S. B. Giddings and S. Thomas, Phys. Rev. D **65**, 056010 (2002) [arXiv:hep-ph/0106219]; S. Dimopoulos and G. Landsberg, Phys. Rev. Lett. **87**, 161602 (2001) [arXiv:hep-ph/0106295]; K. m. Cheung, Phys. Rev. Lett. **88**, 221602 (2002) [arXiv:hep-ph/0110163]; A. Chamblin and G. C. Nayak, Phys. Rev. D **66**, 091901 (2002) [arXiv:hep-ph/0206060].
- [4] E. J. Ahn, M. Cavaglià and A. V. Olinto, Phys. Lett. B **551**, 1 (2003) [arXiv:hep-th/0201042]; E. J. Ahn and M. Cavaglià, Gen. Rel. Grav. **34**, 2037 (2002) [arXiv:hep-ph/0205168]; K. Cheung and C. H. Chou, Phys. Rev. D **66**, 036008 (2002) [arXiv:hep-ph/0205284].
- [5] M. Cavaglià, Int. J. Mod. Phys. A **18**, 1843 (2003) [arXiv:hep-ph/0210296]; G. Landsberg, J. Phys. G **32**, R337 (2006) [arXiv:hep-ph/0607297]; R. Emparan, arXiv:hep-ph/0302226; P. Kanti, Int. J. Mod. Phys. A **19**, 4899 (2004) [arXiv:hep-ph/0402168]; S. Hossenfelder, arXiv:hep-ph/0412265.
- [6] V. Cardoso, E. Berti and M. Cavaglià, Class. Quant. Grav. **22**, L61 (2005) [arXiv:hep-ph/0505125].
- [7] S. W. Hawking, Commun. Math. Phys. **43**, 199 (1975) [Erratum-ibid. **46**, 206 (1976)].
- [8] D. Amati and J. G. Russo, Phys. Lett. B **454**, 207 (1999) [arXiv:hep-th/9901092].
- [9] S. Dimopoulos and G. Landsberg, in *Proc. of the APS/DPF/DPB Summer Study on the Future of Particle Physics (Snowmass 2001)* ed. N. Graf, eConf **C010630**, P321 (2001).
- [10] C. M. Harris, P. Richardson and B. R. Webber, JHEP **0308**, 033 (2003) [arXiv:hep-ph/0307305].
- [11] T. Sjostrand, S. Mrenna and P. Skands, JHEP **0605**, 026 (2006) [arXiv:hep-ph/0603175].
- [12] E. J. Ahn and M. Cavaglià, Phys. Rev. D **73**, 042002 (2006) [arXiv:hep-ph/0511159].
- [13] R. Godang, S. B. Bracker, M. Cavaglià, L. Cremaldi, D. Summers and D. Cline, Int. J. Mod. Phys. A **20**, 3409 (2005) [arXiv:hep-ph/0411248].

[14] K.S. Thorne, in: *Magic without magic: John Archibald Wheeler*, edited by J. Klauder (Freeman, San Francisco, 1972).

[15] M. B. Voloshin, Phys. Lett. B **518**, 137 (2001) [arXiv:hep-ph/0107119]; M. B. Voloshin, Phys. Lett. B **524**, 376 (2002) [Erratum-ibid. B **605**, 426 (2005)] [arXiv:hep-ph/0111099]; T. G. Rizzo, JHEP **0202**, 011 (2002) [arXiv:hep-ph/0201228]; V. S. Rychkov, Phys. Rev. D **70**, 044003 (2004) [arXiv:hep-ph/0401116]; S. B. Giddings and V. S. Rychkov, Phys. Rev. D **70**, 104026 (2004) [arXiv:hep-th/0409131].

[16] H. Yoshino and Y. Nambu, Phys. Rev. D **67**, 024009 (2003) [arXiv:gr-qc/0209003].

[17] H. Yoshino and V. S. Rychkov, Phys. Rev. D **71**, 104028 (2005) [arXiv:hep-th/0503171].

[18] O. I. Vasilenko, arXiv:hep-th/0305067.

[19] P. C. Aichelburg and R. U. Sexl, Gen. Rel. Grav. **2**, 303 (1971).

[20] E. Kohlprath and G. Veneziano, JHEP **0206**, 057 (2002) [arXiv:gr-qc/0203093].

[21] V. Cardoso, O. J. C. Dias and J. P. S. Lemos, Phys. Rev. D **67**, 064026 (2003) [arXiv:hep-th/0212168].

[22] E. Berti, M. Cavaglià and L. Gualtieri, Phys. Rev. D **69**, 124011 (2004) [arXiv:hep-th/0309203].

[23] R. Brock *et al.* [CTEQ Collaboration], Rev. Mod. Phys. **67**, 157 (1995).

[24] W.-M. Yao *et al.* [Particle Data Group], J. Phys. G **33**, 1 (2006).

[25] E. J. Ahn, M. Ave, M. Cavaglià and A. V. Olinto, Phys. Rev. D **68**, 043004 (2003) [arXiv:hep-ph/0306008].

[26] R. Emparan, M. Masip and R. Rattazzi, Phys. Rev. D **65**, 064023 (2002) [arXiv:hep-ph/0109287].

[27] H. Yoshino, T. Shiromizu and M. Shibata, Phys. Rev. D **72**, 084020 (2005) [arXiv:gr-qc/0508063].

[28] M. Cavaglià, S. Das and R. Maartens, Class. Quant. Grav. **20**, L205 (2003) [arXiv:hep-ph/0305223].

[29] M. Cavaglià and S. Das, Class. Quant. Grav. **21**, 4511 (2004) [arXiv:hep-th/0404050].

[30] G. Duffy, C. Harris, P. Kanti and E. Winstanley, JHEP **0509**, 049 (2005) [arXiv:hep-th/0507274]; M. Casals, P. Kanti and E. Winstanley, JHEP **0602**, 051 (2006) [arXiv:hep-th/0511163]; D. Ida, K. y. Oda and S. C. Park, Phys. Rev. D **71**, 124039 (2005) [arXiv:hep-th/0503052]; D. Ida, K. y. Oda and S. C. Park, Phys. Rev. D **73**, 124022 (2006) [arXiv:hep-th/0602188].

[31] P. Kanti and J. March-Russell, Phys. Rev. D **66**, 024023 (2002) [arXiv:hep-ph/0203223]; D. Ida, K. y. Oda and S. C. Park, Phys. Rev. D **67**, 064025 (2003) [Erratum-ibid. D **69**, 049901 (2004)] [arXiv:hep-th/0212108]; P. Kanti and J. March-Russell, Phys. Rev. D **67**, 104019 (2003) [arXiv:hep-ph/0212199]; C. M. Harris and P. Kanti, JHEP **0310**, 014 (2003)

[arXiv:hep-ph/0309054]; C. M. Harris and P. Kanti, Phys. Lett. B **633**, 106 (2006) [arXiv:hep-th/0503010]; E. Jung and D. K. Park, Nucl. Phys. B **731**, 171 (2005) [arXiv:hep-th/0506204]; A. S. Cornell, W. Naylor and M. Sasaki, JHEP **0602**, 012 (2006) [arXiv:hep-th/0510009]; D. K. Park, Phys. Lett. B **638**, 246 (2006) [arXiv:hep-th/0603224].

[32] V. Cardoso, M. Cavaglià and L. Gualtieri, Phys. Rev. Lett. **96**, 071301 (2006) [arXiv:hep-th/0512002]; V. Cardoso, M. Cavaglià and L. Gualtieri, JHEP **0602**, 021 (2006) [arXiv:hep-th/0512116].

[33] M. Cavaglià, Phys. Lett. B **569**, 7 (2003) [arXiv:hep-ph/0305256].

[34] A. Chamblin, F. Cooper and G. C. Nayak, Phys. Rev. D **70**, 075018 (2004) [arXiv:hep-ph/0405054].

[35] V. P. Frolov and D. Stojkovic, Phys. Rev. D **66**, 084002 (2002) [arXiv:hep-th/0206046].

[36] L. J. Garay, Int. J. Mod. Phys. A **10**, 145 (1995) [arXiv:gr-qc/9403008].

[37] M. Acciarri *et al.* [L3 Collaboration], Phys. Lett. B **470**, 268 (1999) [arXiv:hep-ex/9910009]; G. Abbiendi *et al.* [OPAL Collaboration], Eur. Phys. J. C **18**, 253 (2000) [arXiv:hep-ex/0005002]; A. Heister *et al.* [ALEPH Collaboration], Eur. Phys. J. C **28**, 1 (2003); P. Abreu *et al.* [DELPHI Collaboration], Phys. Lett. B **485**, 45 (2000) [arXiv:hep-ex/0103025].; V. M. Abazov *et al.* [D0 Collaboration], Phys. Rev. Lett. **90**, 251802 (2003) [arXiv:hep-ex/0302014]; D. Acosta [CDF Collaboration], Phys. Rev. Lett. **92**, 121802 (2004) [arXiv:hep-ex/0309051].

[38] V. D. Barger, T. Han, C. Kao and R. J. Zhang, Phys. Lett. B **461**, 34 (1999) [arXiv:hep-ph/9905474]; S. Hannestad and G. Raffelt, Phys. Rev. Lett. **87**, 051301 (2001) [arXiv:hep-ph/0103201]; S. Hannestad and G. G. Raffelt, Phys. Rev. Lett. **88**, 071301 (2002) [arXiv:hep-ph/0110067]; M. Fairbairn, Phys. Lett. B **508**, 335 (2001) [arXiv:hep-ph/0101131]; L. J. Hall and D. R. Smith, Phys. Rev. D **60**, 085008 (1999) [arXiv:hep-ph/9904267].

[39] L. Randall and R. Sundrum, Phys. Rev. Lett. **83**, 4690 (1999) [arXiv:hep-th/9906064]; L. Randall and R. Sundrum, Phys. Rev. Lett. **83**, 3370 (1999) [arXiv:hep-ph/9905221].

[40] H. L. Lai *et al.* [CTEQ Collaboration], “Global QCD analysis of parton structure of the nucleon: CTEQ5 parton Eur. Phys. J. C **12**, 375 (2000) [arXiv:hep-ph/9903282].

[41] B. Koch, M. Bleicher and S. Hossenfelder, JHEP **0510**, 053 (2005) [arXiv:hep-ph/0507138].

[42] H. Stocker, arXiv:hep-ph/0605062.

[43] C. M. Harris, M. J. Palmer, M. A. Parker, P. Richardson, A. Sabetfakhri and B. R. Webber, JHEP **0505**, 053 (2005) [arXiv:hep-ph/0411022]; B. Webber, eConf **C0507252**, T030 (2005) [arXiv:hep-ph/0511128].

[44] G. L. Alberghi, R. Casadio, D. Galli, D. Gregori, A. Tronconi and V. Vagnoni, arXiv:hep-ph/0601243.

[45] J. Tanaka, T. Yamamura, S. Asai and J. Kanzaki, Eur. Phys. J. C **41**, 19 (2005) [arXiv:hep-ph/0411095].

- [46] L. Lonnblad, M. Sjodahl and T. Akesson, JHEP **0509**, 019 (2005) [arXiv:hep-ph/0505181].
- [47] G. C. Nayak and J. Smith, Phys. Rev. D **74**, 014007 (2006) [arXiv:hep-ph/0602129].
- [48] M. Cavaglià *et. al.*, in preparation.
- [49] J. D. Bjorken and S. J. Brodsky, Phys. Rev. D **1**, 1416 (1970).
- [50] S. Brandt, C. Peyrou, R. Sosnowski and A. Wroblewski, Phys. Lett. **12**, 57 (1964).
- [51] G. C. Fox and S. Wolfram, Phys. Rev. Lett. **41**, 1581 (1978); Nucl. Phys. B **149**, 413 (1979) [Erratum-ibid. B **157**, 543 (1979)].
- [52] L. Anchordoqui and H. Goldberg, Phys. Rev. D **67**, 064010 (2003) [arXiv:hep-ph/0209337]; A. Casanova and E. Spallucci, Class. Quant. Grav. **23**, R45 (2006) [arXiv:hep-ph/0512063].

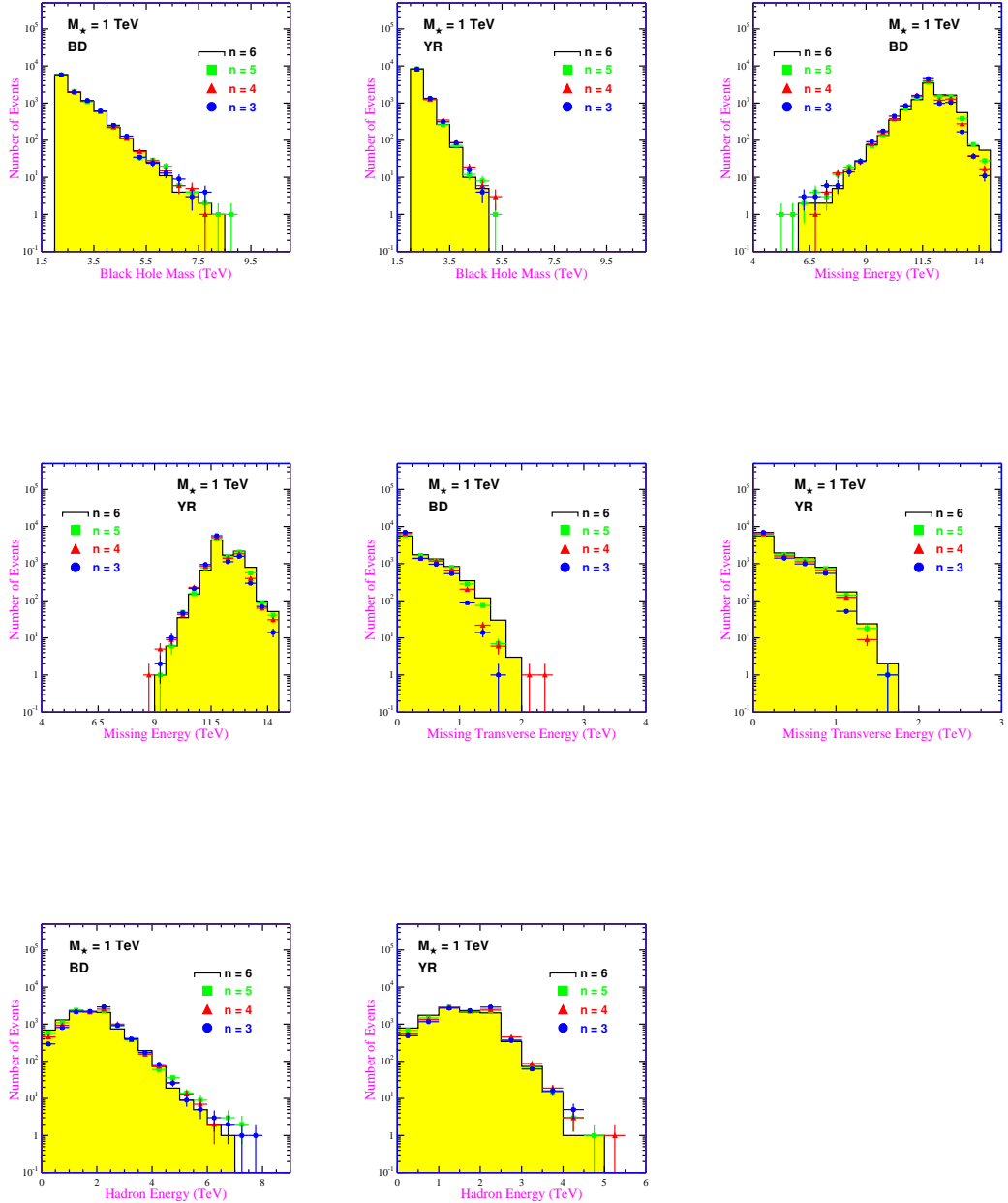


Figure 1: M_{BH} distribution, \cancel{E} , \cancel{E}_T and E_H for the black disk model (BD) and the Yoshino-Rychkov TS model (YR) and number of extra dimensions $n = 3 \dots 6$. The fundamental Planck scale M_{\star} is 1 TeV.

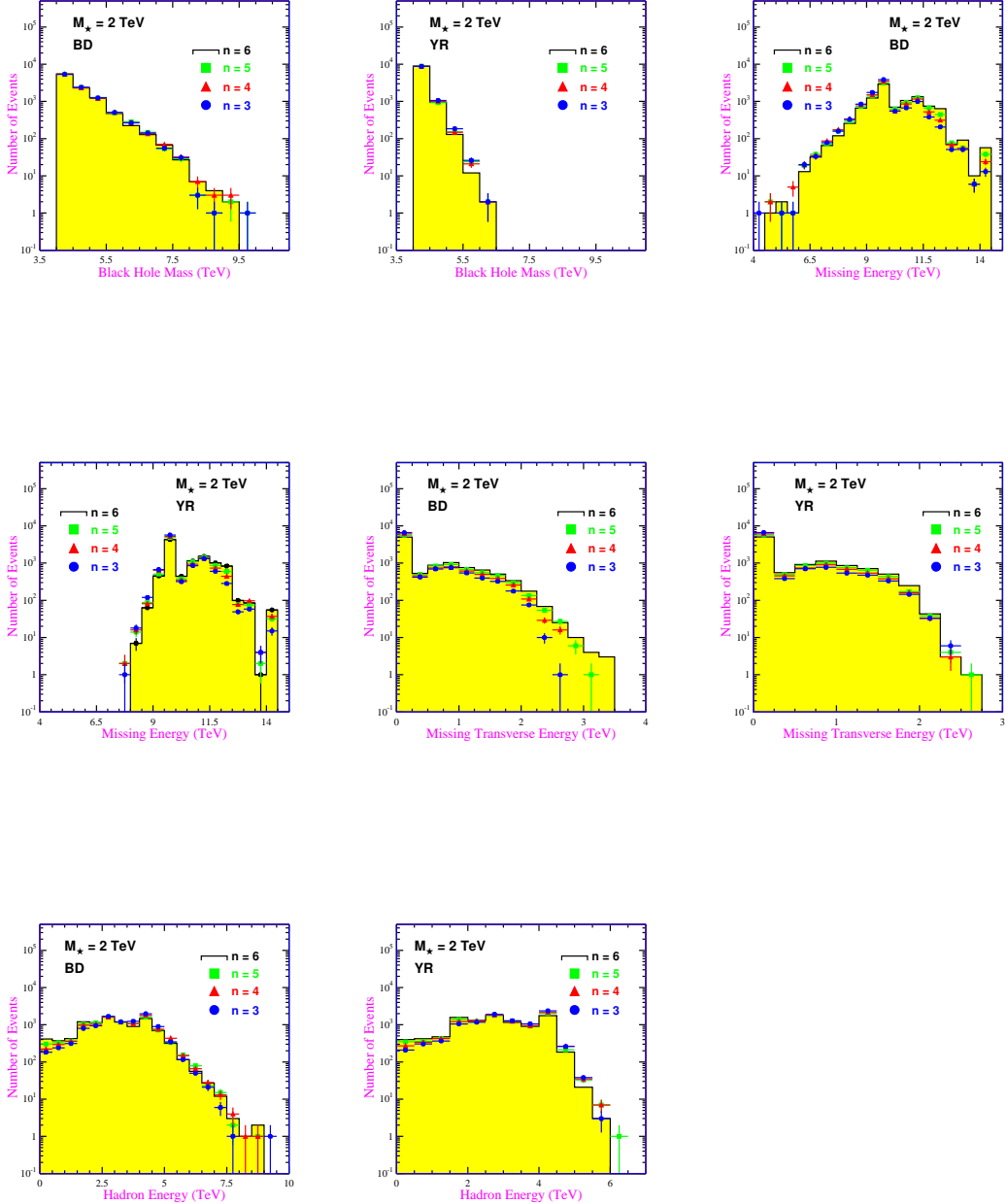


Figure 2: M_{BH} distribution, \cancel{E} , \cancel{E}_T and E_H for the black disk model (BD) and the Yoshino-Rychkov TS model (YR) and number of extra dimensions $n = 3 \dots 6$. The fundamental Planck scale M_\star is 2 TeV.

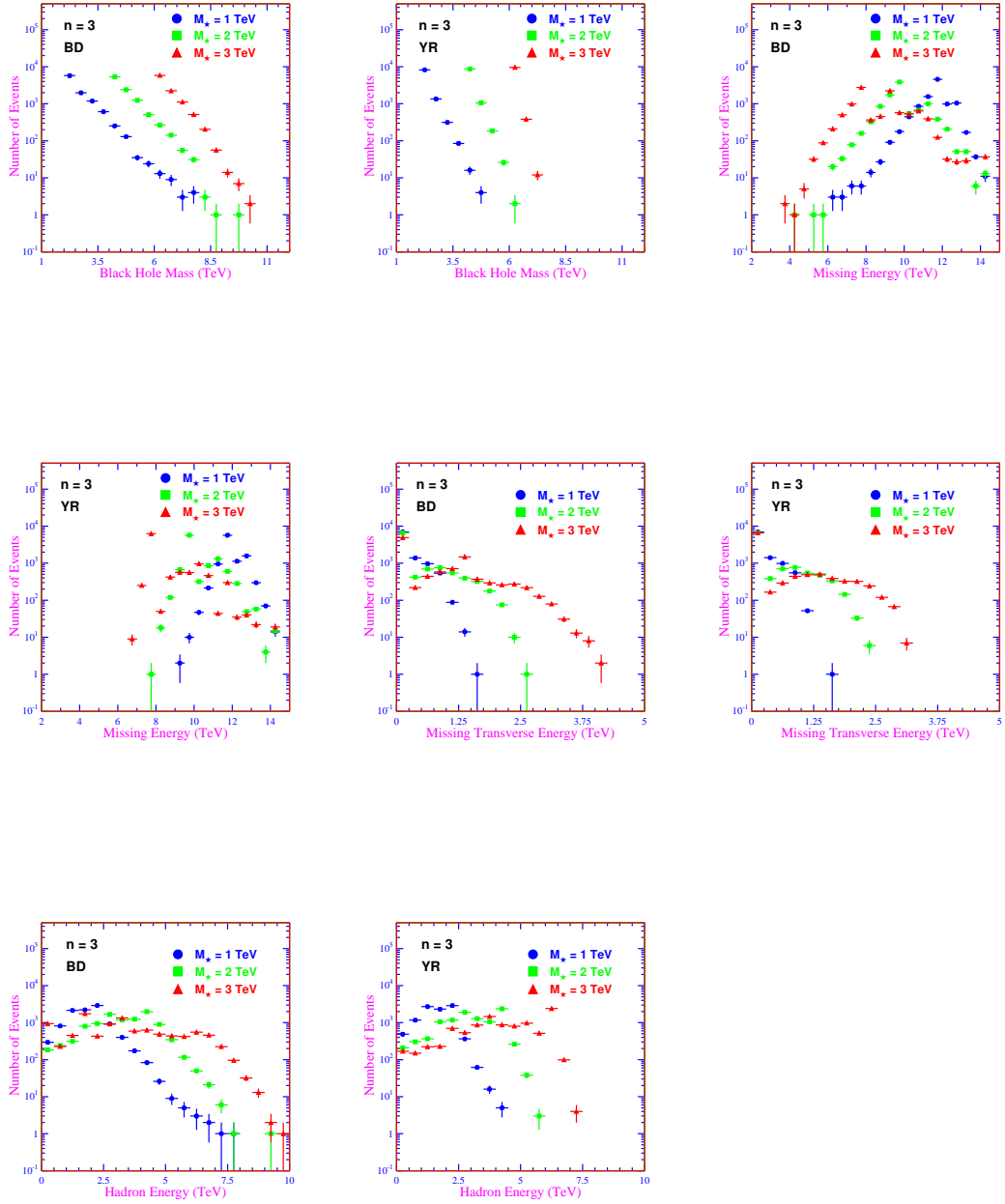


Figure 3: M_{BH} , \cancel{E} , \cancel{E}_T and E_H for the black disk model (BD) and the Yoshino-Rychkov TS model (YR) in a six-dimensional spacetime ($n = 3$) with fundamental Planck scale $M_\star = 1, 2$ and 3 TeV.

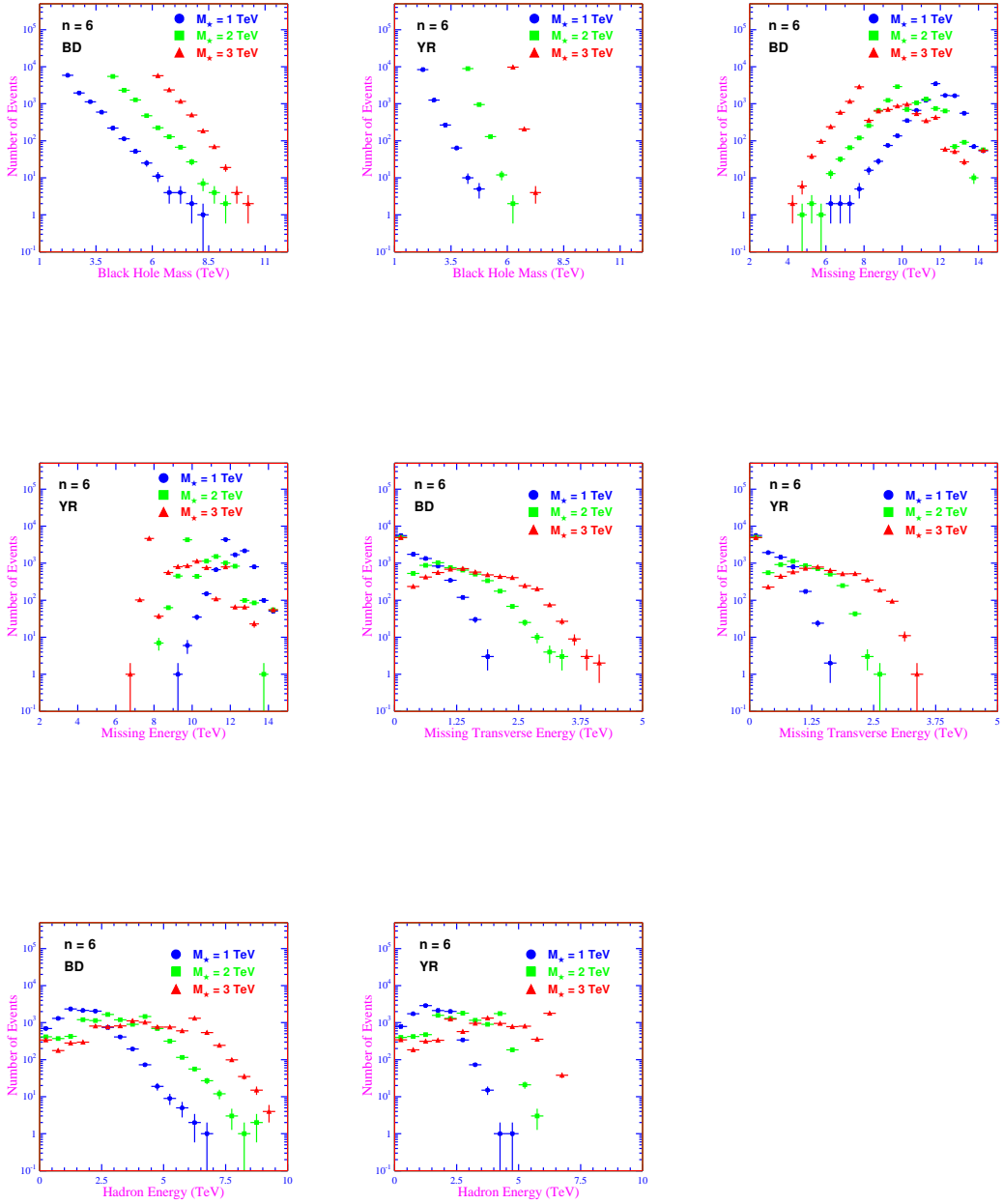


Figure 4: M_{BH} , \cancel{E} , \cancel{E}_T and E_H for the black disk model (BD) and the Yoshino-Rychkov TS model (YR) in a ten-dimensional spacetime ($n = 6$) with fundamental Planck scale $M_\star = 1, 2$ and 3 TeV.

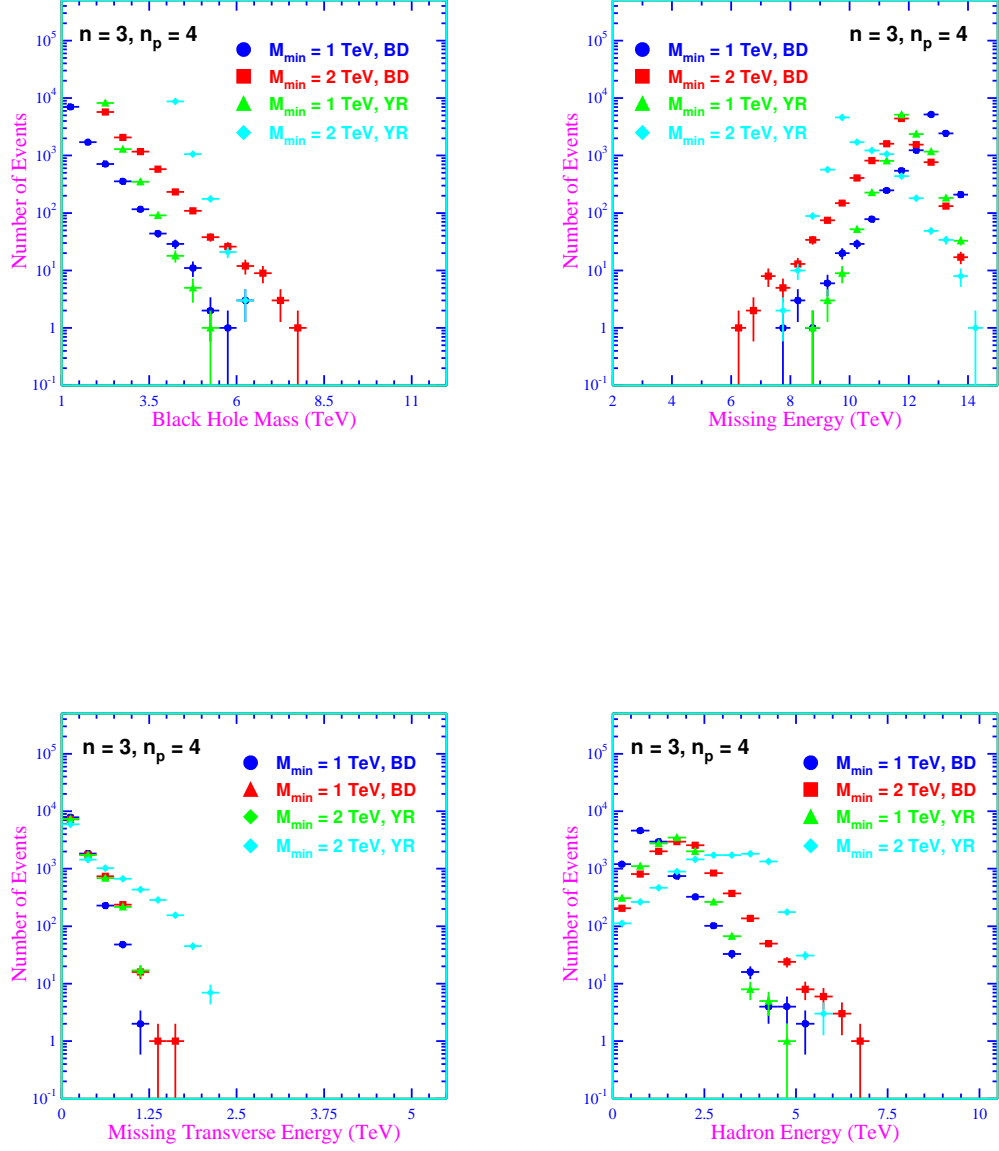


Figure 5: M_{BH} , \cancel{E} , \cancel{E}_T and E_H for the black disk model (BD) and the Yoshino-Rychkov TS model (YR) in a six-dimensional spacetime ($n = 3$) with fundamental Planck scale $M_\star = 1$ TeV. The minimum formation mass of the BH is $M_{min} = 1$ TeV or $M_{min} = 2$ TeV. The final BH decay is in four hard quanta ($n_p = 4$).

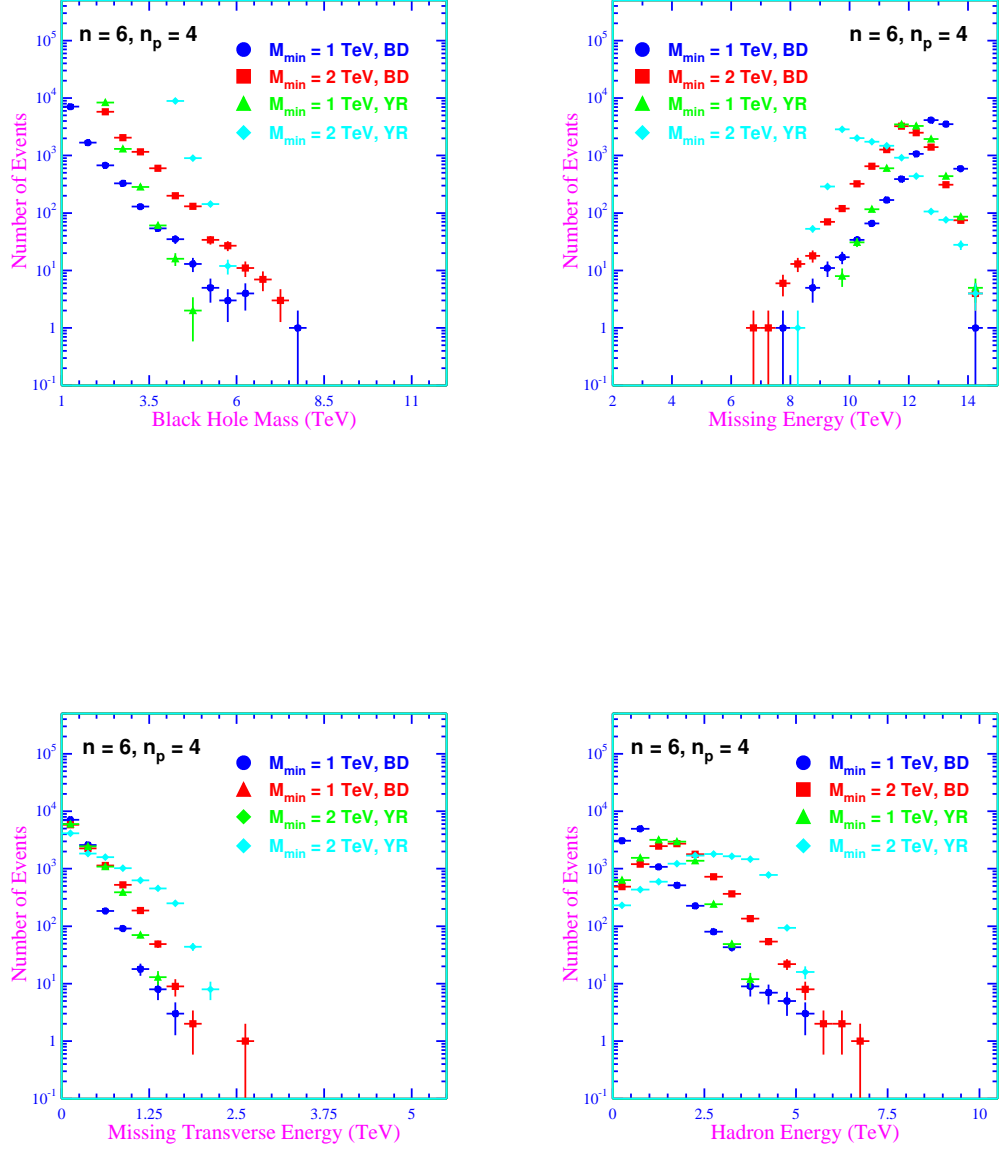


Figure 6: M_{BH} , \cancel{E} , \cancel{E}_T and E_H for the black disk model (BD) and the Yoshino-Rychkov TS model (YR) in a ten-dimensional spacetime ($n = 6$) with fundamental Planck scale $M_\star = 1$ TeV. The minimum formation mass of the BH is $M_{min} = 1$ TeV or $M_{min} = 2$ TeV. The final BH decay is in four hard quanta ($n_p = 4$).

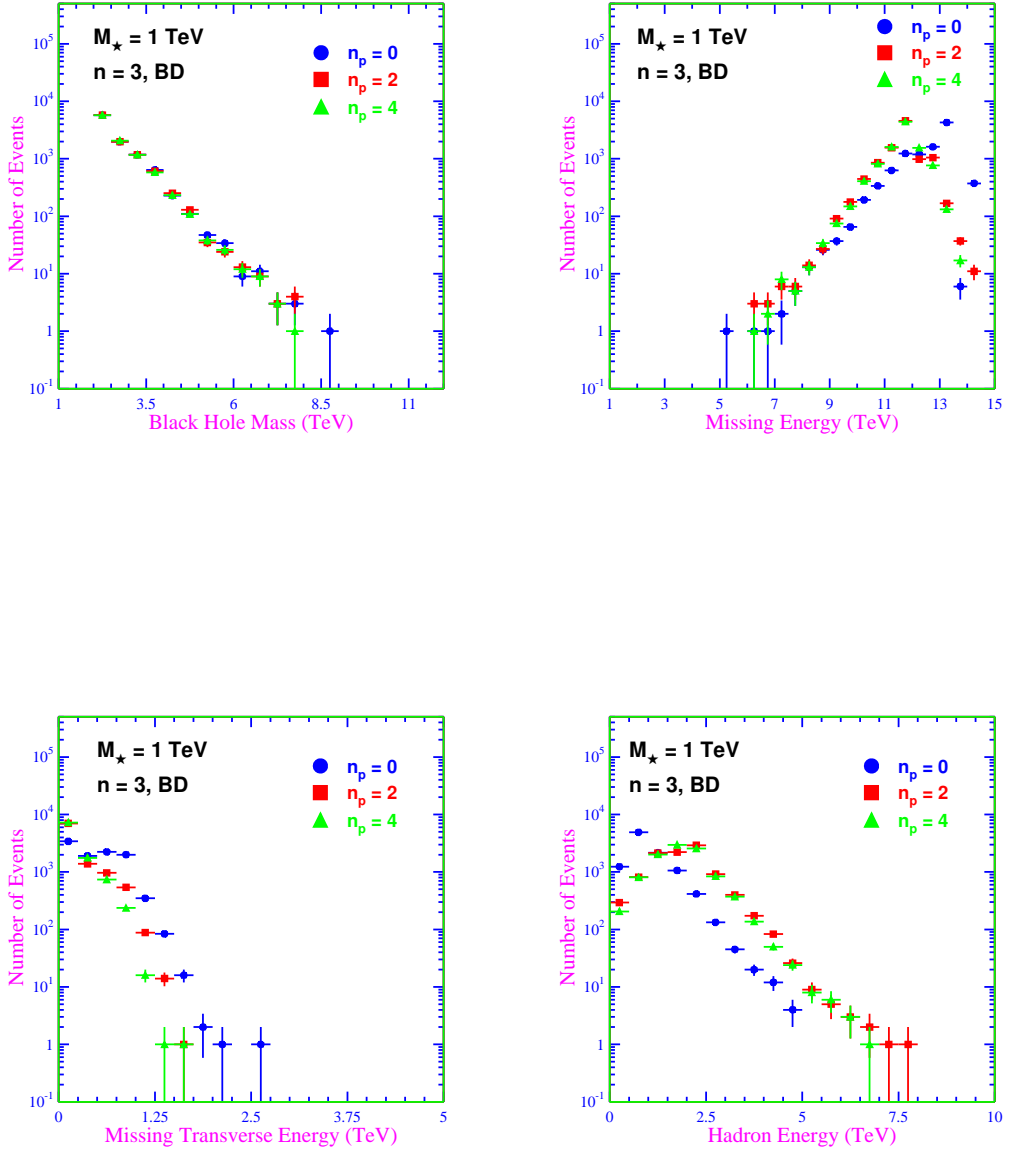


Figure 7: M_{BH} , \mathcal{E} , \mathcal{E}_T and E_H for the black disk model (BD) model in a six-dimensional spacetime ($n = 3$) with fundamental Planck scale $M_* = 1$ TeV and different final decay modes: neutral remnant ($n_p = 0$), two hard quanta ($n_p = 2$) and four hard quanta ($n_p = 4$).

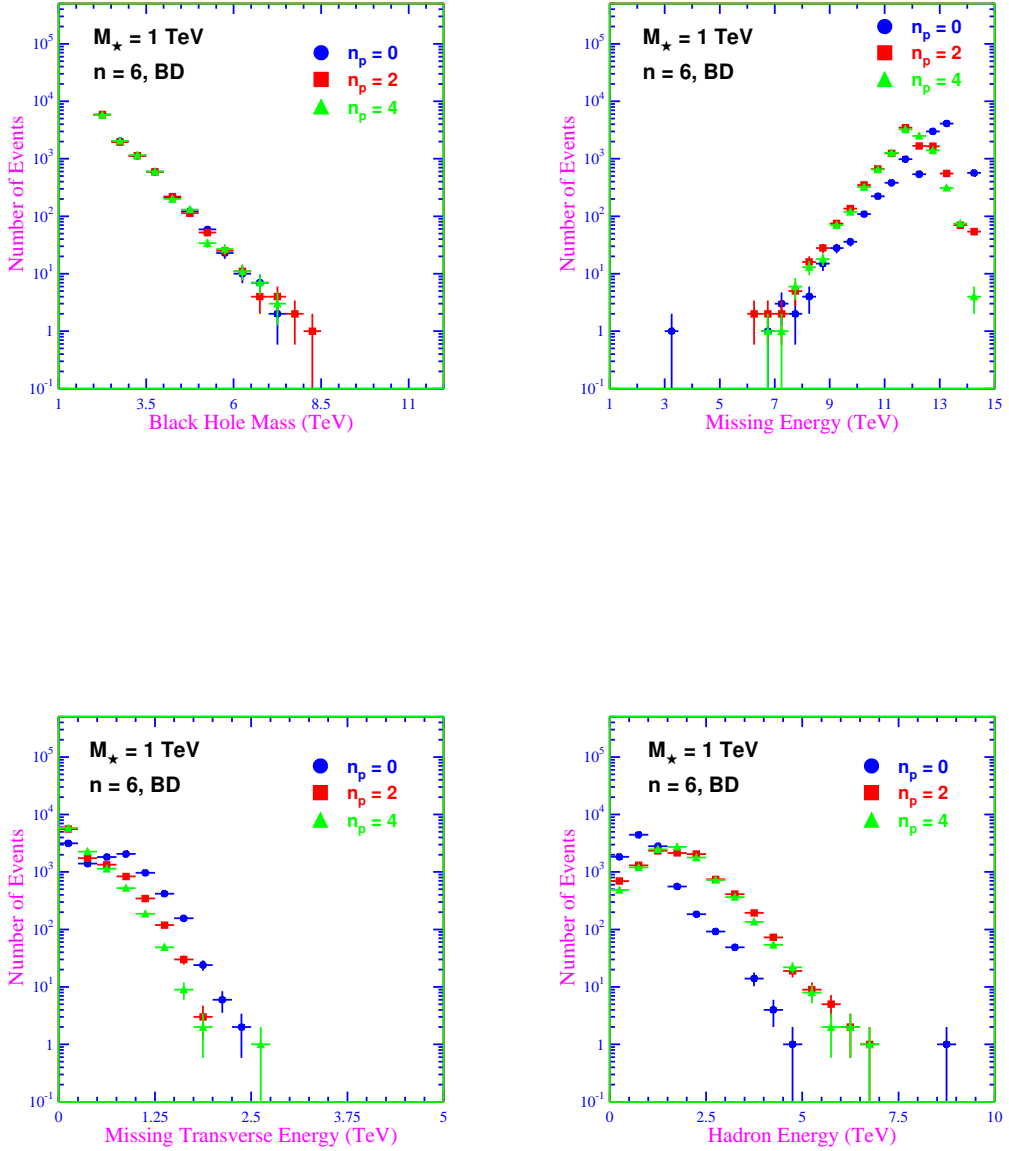


Figure 8: M_{BH} , \cancel{E} , \cancel{E}_T and E_H for the black disk model (BD) in a ten-dimensional spacetime ($n = 6$) with fundamental Planck scale $M_* = 1$ TeV and different final decay modes: neutral remnant ($n_p = 0$), two hard quanta ($n_p = 2$) and four hard quanta ($n_p = 4$).

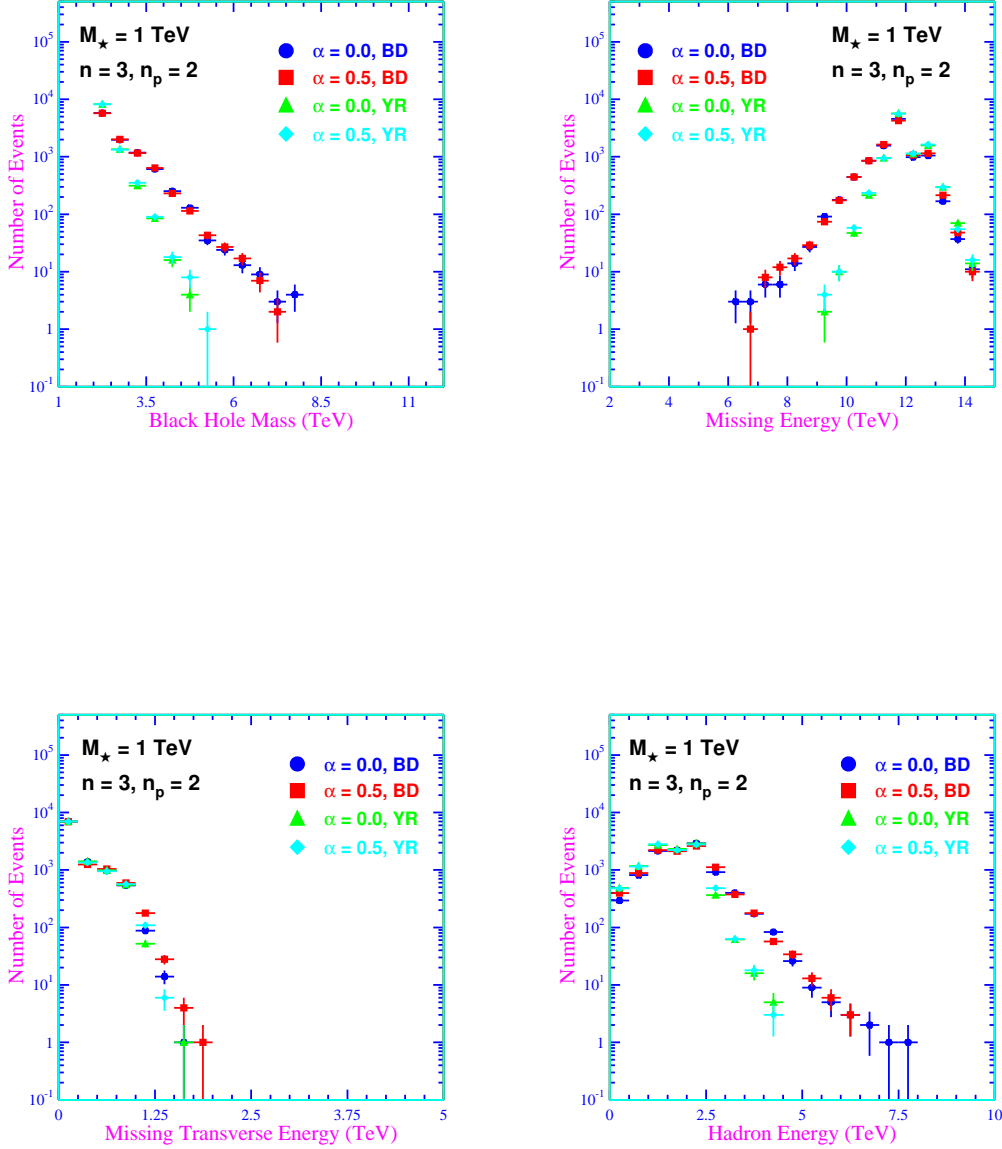


Figure 9: M_{BH} , \cancel{E} , \cancel{E}_T and E_H for the black disk model (BD) and the Yoshino-Rychkov TS model (YR) in a six-dimensional spacetime ($n = 3$) with fundamental Planck scale $M_\star = 1$ TeV and zero ($\alpha = 0$) or M_\star^{-1} ($\alpha = 0.5$) minimum length. The final BH decay is in two hard quanta.

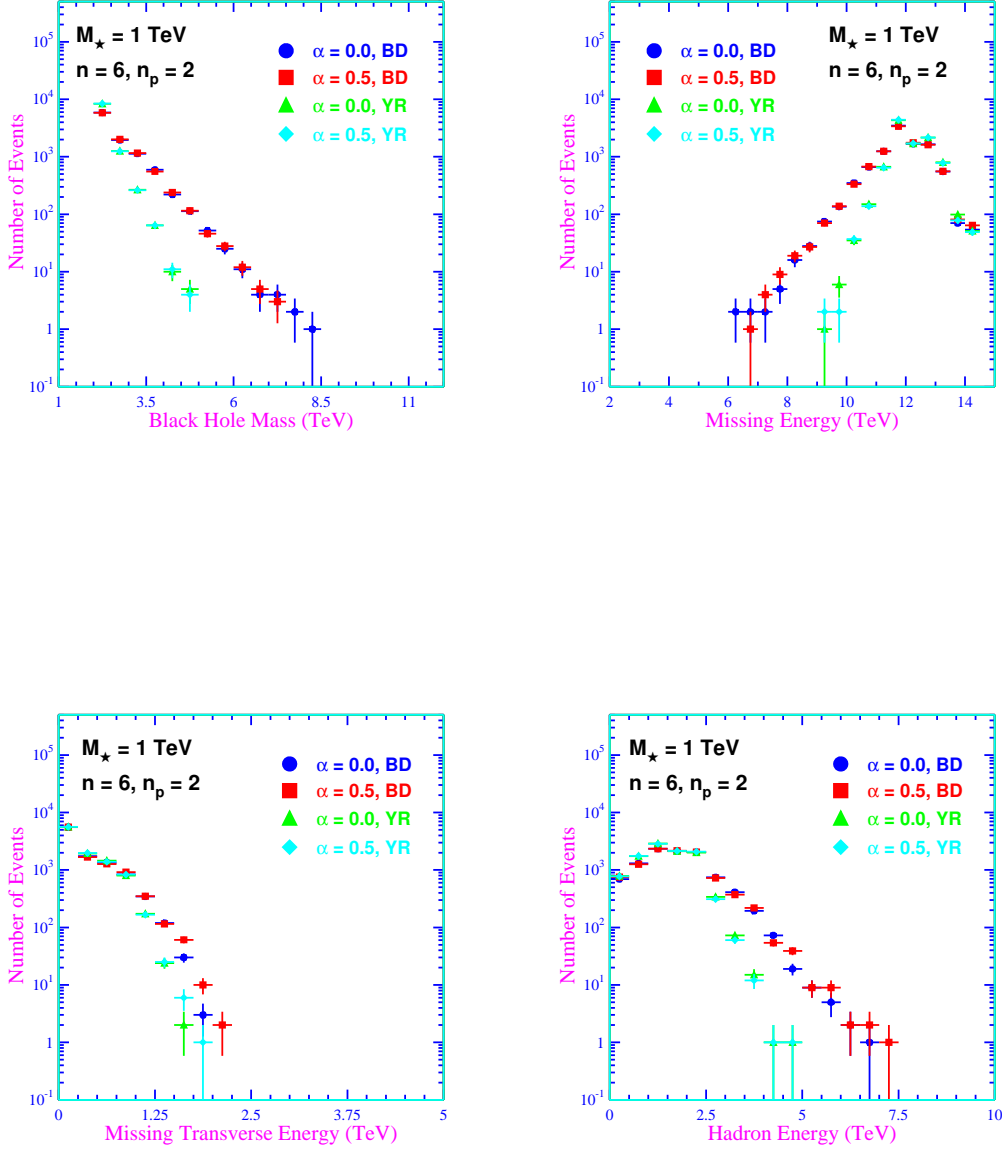


Figure 10: M_{BH} , \mathcal{E} , \mathcal{E}_T and E_H for the black disk model (BD) and the Yoshino-Rychkov TS model (YR) in a ten-dimensional spacetime ($n = 6$) with fundamental Planck scale $M_* = 1$ TeV and zero ($\alpha = 0$) or M_*^{-1} ($\alpha = 0.5$) minimum length. The final BH decay is in two hard quanta.

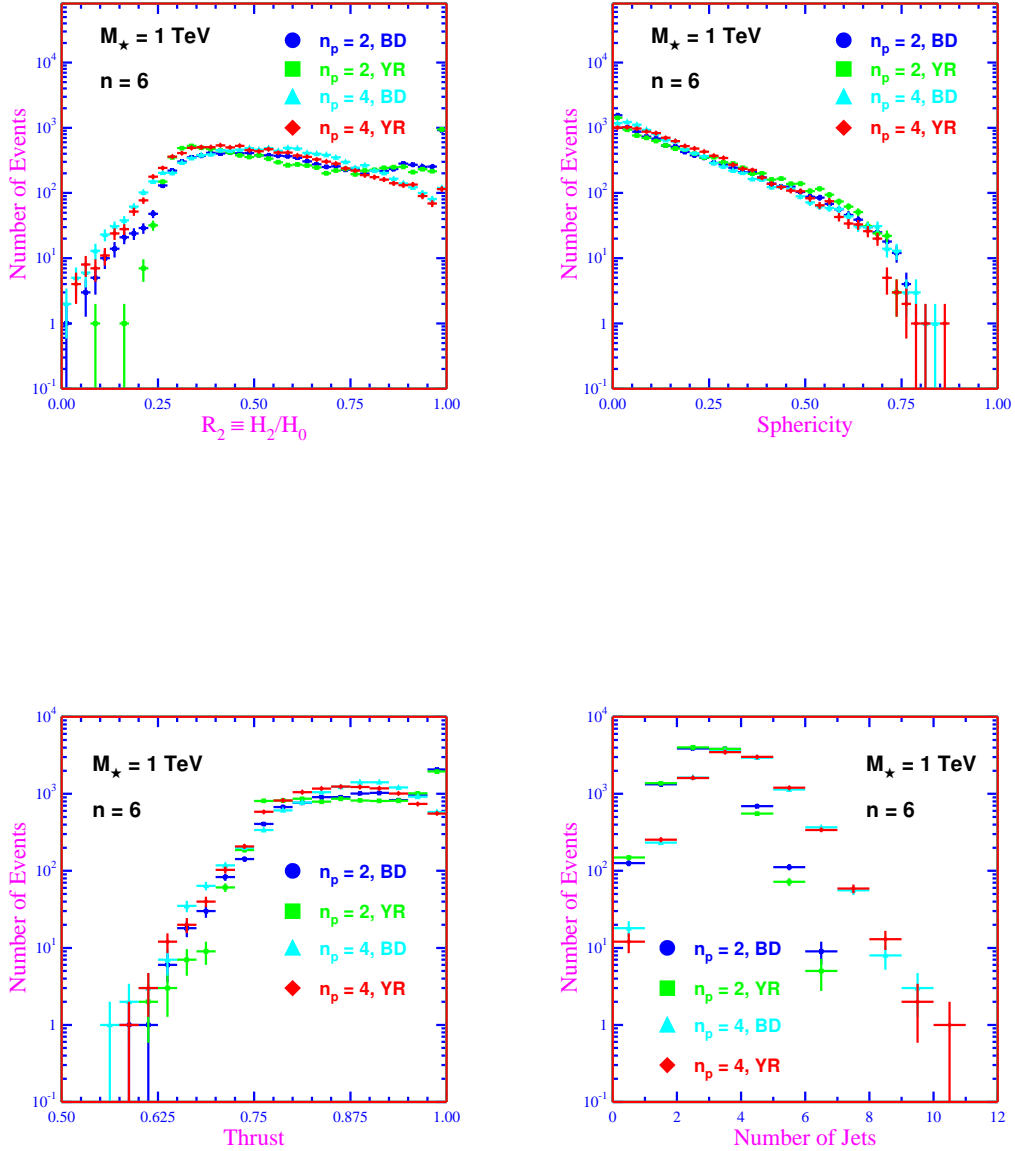


Figure 11: Fox-Wolfram moment R_2 , sphericity, thrust and number of jets for the black disk model (BD) and the Yoshino-Rychkov TS model (YR) in a ten-dimensional spacetime ($n = 6$). The final black hole decay is in two hard quanta ($n_p = 2$) or four hard quanta ($n_p = 4$).

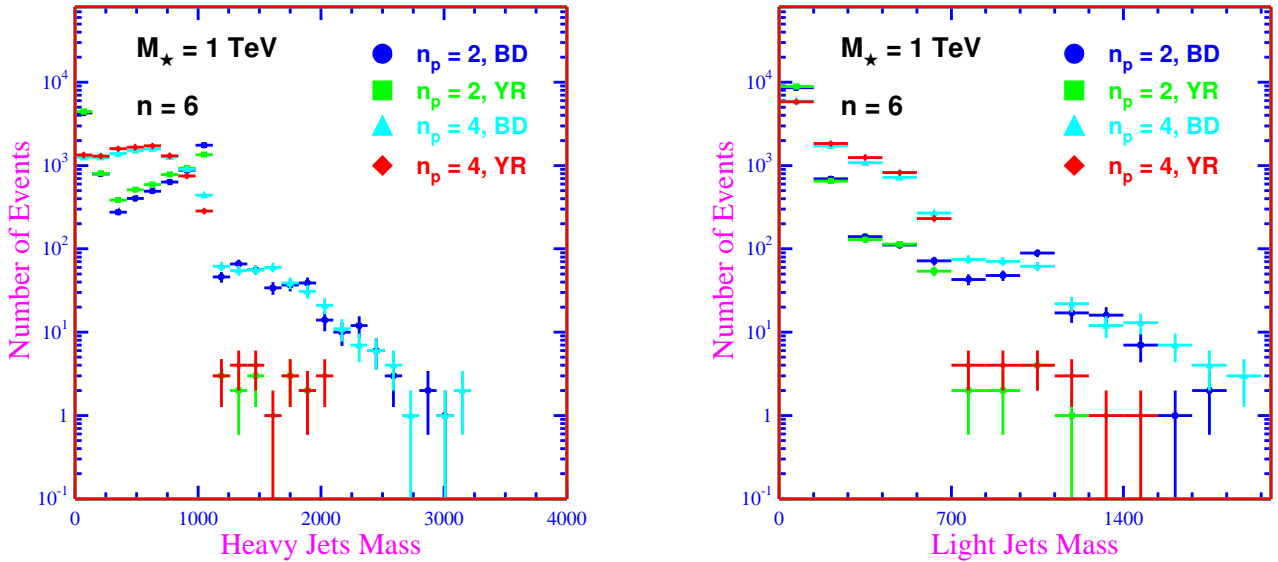


Figure 12: Heavy and light jet mass for the black disk model (BD) and the Yoshino-Rychkov TS model (YR) in a ten-dimensional spacetime ($n = 6$). The final black hole decay is in two hard quanta ($n_p = 2$) or four hard quanta ($n_p = 4$).